AIP Conference Proceedings

A high-accuracy calibration method for temperature dependent photoluminescence imaging

Cite as: AIP Conference Proceedings **2147**, 020007 (2019); https://doi.org/10.1063/1.5123812
Published Online: 27 August 2019

Sissel Tind Kristensen, Shuai Nie, Marie Syre Wiig, Halvard Haug, Charly Berthod, Rune Strandberg, and Ziv Hameiri

View Online

Export Citation

ARTICLES YOU MAY BE INTERESTED IN

Accurate contact and contactless methods for emitter sheet resistance testing of PV wafers
AIP Conference Proceedings **2147**, 020006 (2019); https://doi.org/10.1063/1.5123811

Characterization of absorption losses in rear side n-type polycrystalline silicon passivating contacts
AIP Conference Proceedings **2147**, 040004 (2019); https://doi.org/10.1063/1.5123831

Study of non fire-through metallization processes of boron-doped polysilicon passivated contacts for high efficiency silicon solar cells
AIP Conference Proceedings **2147**, 040006 (2019); https://doi.org/10.1063/1.5123833

Lock-in Amplifiers up to 600 MHz
starting at
$6,210

AIP Publishing

© 2019 Author(s).

A High-Accuracy Calibration Method for Temperature Dependent Photoluminescence Imaging

Sissel Tind Kristensen[1,a)], Shuai Nie[2], Marie Syre Wiig[3], Halvard Haug[3], Charly Berthod[1], Rune Strandberg[1], and Ziv Hameiri[2]

[1]University of Agder, Jon Lilletunsvei 9, 4879 Grimstad, Norway
[2]University of New South Wales, 229 Anzac Parade, 2052, Sydney, NSW, Australia
[3]Institute for Energy Technology, Instituttveien 18, 2007 Kjeller, Norway

[a)]Corresponding author: sissel.t.kristensen@uia.no

Abstract. This work demonstrates a novel technique for calibrating temperature dependent photoluminescence (PL) images of silicon wafers with high accuracy. The PL signal is calibrated using a heat-controlled photoconductance (PC) stage integrated into the PL imaging system. The PC signal is measured in true steady state condition and used to determine the calibration constant under the same temperature and illumination as the PL image, thus providing a high-precision calibration. This results in a robust method for imaging of important physical parameters, such as the minority carrier lifetime and the implied voltage at different temperatures, as well as the temperature coefficients and the recombination parameter γ. The method is verified through comparison with a similar PL imaging system, where the calibration is made from a conventional flash-based quasi-steady-state PC measurement. Finally, the method is applied to compensated multicrystalline silicon wafers, demonstrating the usefulness of the proposed calibration routine for analysing complex materials.

INTRODUCTION

Photoluminescence (PL) imaging is a spatially resolved measurement technique enabling fast acquisition of important parameters for silicon wafers and cells [1]. Of these, a key parameter is the minority carrier lifetime [2], which is essential for estimating the final performance of a solar cell.

In the later years, the interest in PL imaging at elevated temperatures has increased, since knowledge about the temperature sensitivity of a material can unlock important information about the material properties [3-6]. In addition, it can give a more accurate representation of the performance of a photovoltaic device under real operating conditions, where temperatures can differ significantly from the standard test condition (STC) temperature of 25 °C [7].

Calibration of temperature dependent PL images is a complex task. This is due to a strong temperature dependence of the luminescence signal from a silicon sample, originating from the temperature dependence of the radiative recombination coefficient, the optical properties of the sample, the spectral distribution of the luminescence signal, and the temperature sensitivity of the camera [8]. Current calibration procedures for elevated temperatures include modelling [3], purely optical measurement techniques utilizing the time dependence of the luminescence signal [4], or calibration by temperature dependent quasi-steady-state (QSS) photo-conductance (PC) measurements [5]. A QSS-PC based calibration is the most accessible option in many laboratories since it requires only standard equipment and carry limited assumptions. However, some uncertainties might be introduced since the calibration process and image acquisition are conducted on separate systems [5].

In this paper, we present a calibration routine based on a direct measurement of the PC of a wafer during PL image acquisition. The calibration parameters are therefore obtained under similar temperature and illumination conditions as the PL image, resulting in a high-precision calibration with even fewer assumptions.

SiliconPV 2019, the 9th International Conference on Crystalline Silicon Photovoltaics
AIP Conf. Proc. 2147, 020007-1–020007-6; https://doi.org/10.1063/1.5123812
Published by AIP Publishing. 978-0-7354-1892-9/$30.00

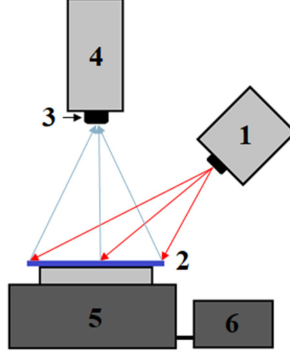

FIGURE 1. Illustration of the temperature dependent PL imaging setup (System I) consisting of: (1) 808 nm laser diode; (2) sample; (3) objective and filters; (4) Si CCD camera; (5) combined PC and heat stage; (6) temperature-controller.

EXPERIMENTAL METHOD

Figure 1 illustrates the measurement setup consisting of a temperature-controlled PC stage integrated into a PL imaging system. The PL imaging system consists of an 808 nm laser for excitation of the wafer and a silicon charge-coupled device (CCD) camera for collection of the PL signal emitted from the wafer. Several filters are attached in front of the camera to remove reflections of the laser beam and reflections of the PL signal originating from the stage. The collected PL signal from the wafer, I_{PL}, can be expressed as

$$I_{\mathrm{PL}} = A_i B\, \Delta n \left(\Delta n + N_{\mathrm{dop}} \right) \tag{1}$$

where A_i is a constant depending on the specific PL measurement system and sample, B denotes the radiative recombination coefficient [8], Δn is the excess carrier density, and N_{dop} is the bulk doping concentration.

The temperature-controlled PC stage (Sinton Instruments WCT-120TS [9]) measures the conductance of the wafer using an inductive coil, thus allowing a direct measure of the PC during image acquisition in true steady-state at any desired temperature from 25°C to 200°C. Note that the temperature was kept at maximum 75°C during our experiments to prevent the equipment from heating up and to avoid permanent changes in the carrier lifetime of the wafers. Using a suitable mobility model applied at the specific conditions of image acquisition, the measured PC, $\Delta\sigma$, can be translated into an average Δn in the coil area of the wafer, Δn_{PC}, using [10]

$$\Delta n_{\mathrm{PC}} = \frac{\Delta\sigma}{qW\mu_{\mathrm{tot}}} \tag{2}$$

where q denotes the elementary charge, W is the thickness of the silicon wafer, and μ_{tot} is the sum of the mobilities of electrons and holes in the material. Combining Eqs. (1) and (2) and assuming that Δn_{PC} equals the average Δn in the coil area of the PL image, the calibration constants $A_i B$ can be determined. Hence, Δn can be obtained for each pixel of the PL image. This allows for a high-accuracy conversion of the PL images into images of important device parameters, such as the effective minority carrier lifetime, τ_{eff}, and the implied open circuit voltage, iV_{oc}. In steady-state, τ_{eff} is directly proportional to Δn and can be calculated using $\tau_{\mathrm{eff}} = \Delta n/G$ where G is the generation rate. The iV_{oc} can be determined from Δn using [10]

$$V_{\mathrm{oc}} = \frac{kT_{\mathrm{c}}}{q} \ln\left(\frac{\Delta n \left(\Delta n + N_{\mathrm{dop}} \right)}{n_i^2} \right) \tag{3}$$

where k denotes Boltzmann's constant, T_{c} is the temperature of the cell, and n_i is the intrinsic carrier concentration at the specific temperature of interest.

Following the method described in Ref. [6], additional maps can be generated displaying the temperature coefficient of iV_{oc}, β_{iVoc}, and the recombination parameter γ, related to V_{oc} through [11]

$$\beta_{V_{oc}} = \frac{dV_{oc}}{dT_c} = -\frac{E_{g0}/q - V_{oc} + \gamma k T_c/q}{T_c} \tag{4}$$

where E_{g0} is the semiconductor bandgap energy extrapolated to 0 K. The parameter γ includes the temperature dependence of the dark saturation current, J_0, and gives information regarding the dominating recombination mechanism in the material [7]. This setup will be referred to as 'System I' hereafter.

To verify the method, the wafers were characterized using a similar PL imaging system, but with a calibration process performed on a separate PC system (also a WCT-120TS from Sinton Instruments) following Ref. [5]. The calibration is based on conventional QSS-flash lifetime curves acquired at different temperatures to obtain Δn_{PC} and τ_{eff} at comparable generation conditions as the PL images. The obtained τ_{eff} is then assumed to equal the average τ_{eff} in the coil area of the PL image. The setup will be referred to as 'System II' hereafter. A constant photon flux of 1.2×10^{17} cm^{-2} s^{-1} was used for excitation in both Systems I and II.

Two different wafers were characterized to compare Systems I and II: Wafer A) a 2" n-type monocrystalline silicon (mono-Si) wafer with a resistivity of 3-4 Ω·cm and passivated with an aluminum oxide (AlO_x) and silicon nitride (SiN_x) stack layer, and Wafer B) a 6" p-type multicrystalline silicon (mc-Si) wafer with a resistivity of 2-3 Ω·cm passivated with SiN_x. The wafers were characterized using both systems within a period of three weeks. The stability of the wafers was monitored using a WCT-120TS lifetime tester. A third and fourth wafer were used for application of System I: Two 6" compensated p-type mc-Si wafers originating from the same central brick of a compensated ingot containing boron, gallium and phosphorus, with a resistivity of 1-2 Ω·cm. Wafer C) was taken from the bottom of the brick at a relative height of 0.06, while Wafer D) was taken from the top of the brick at a relative height of 0.82. Both wafers were passivated with hydrogenated amorphous silicon (a-Si:H) and SiN_x.

RESULTS AND DISCUSSION

Verification: Average and Spatial Comparison

The average τ_{eff} in the PC coil area of the PL image of Wafer A and Wafer B can be seen in Figs. 2(a) and (c), respectively, as a function of temperature measured on both systems. The errors on System I are estimated based on the uncertainty of the PC measurement and the repeatability of the system, the former found to have the biggest impact on the calibrated lifetime. The errors on System II are estimated based on repeatability of the lifetime measurement. The errors thus represent minimum uncertainties associated with the Systems I and II. A good agreement within the estimated errors is observed when comparing the two systems. System II displays slightly lower average τ_{eff} for Wafer A compared to System I, however, the variation is within the estimated minimum errors. The temperature sensitivity of τ_{eff} shows similar trends on both systems for both wafers.

To investigate the spatial distribution across the wafers, histograms were created to examine the number of pixels with different lifetimes. This is shown in Figs. 2(b) and (d) for Wafers A and B, respectively, measured on both systems at 55°C. A similar shape of distributions can be observed on the two systems; However, System II is found to exhibit a slightly narrower distribution compared to System I and an increased number of high-lifetime pixels for both wafers. This could be a consequence of differences in reflection from the PC coil area in the two systems, causing a larger contrast in the PL signal around the coil area of System I (visible on raw PL images of the mono-wafer). Note that the lifetimes of Wafer A measured on System II are shifted to slightly lower values compared to System I, as expected from the average values.

Good agreement is found between both calibration procedures for the studied samples, and System I can be considered a further development of System II with a more robust calibration routine. The new calibration is performed directly in the PL system under true steady-state condition using the same illumination and temperature as the PL image resulting in fewer possible errors. Furthermore, both Systems I and II obtain their calibration constants by correlating the measured PC signal of the wafer with the location of the PC coil in the PL image. Since the PC stage

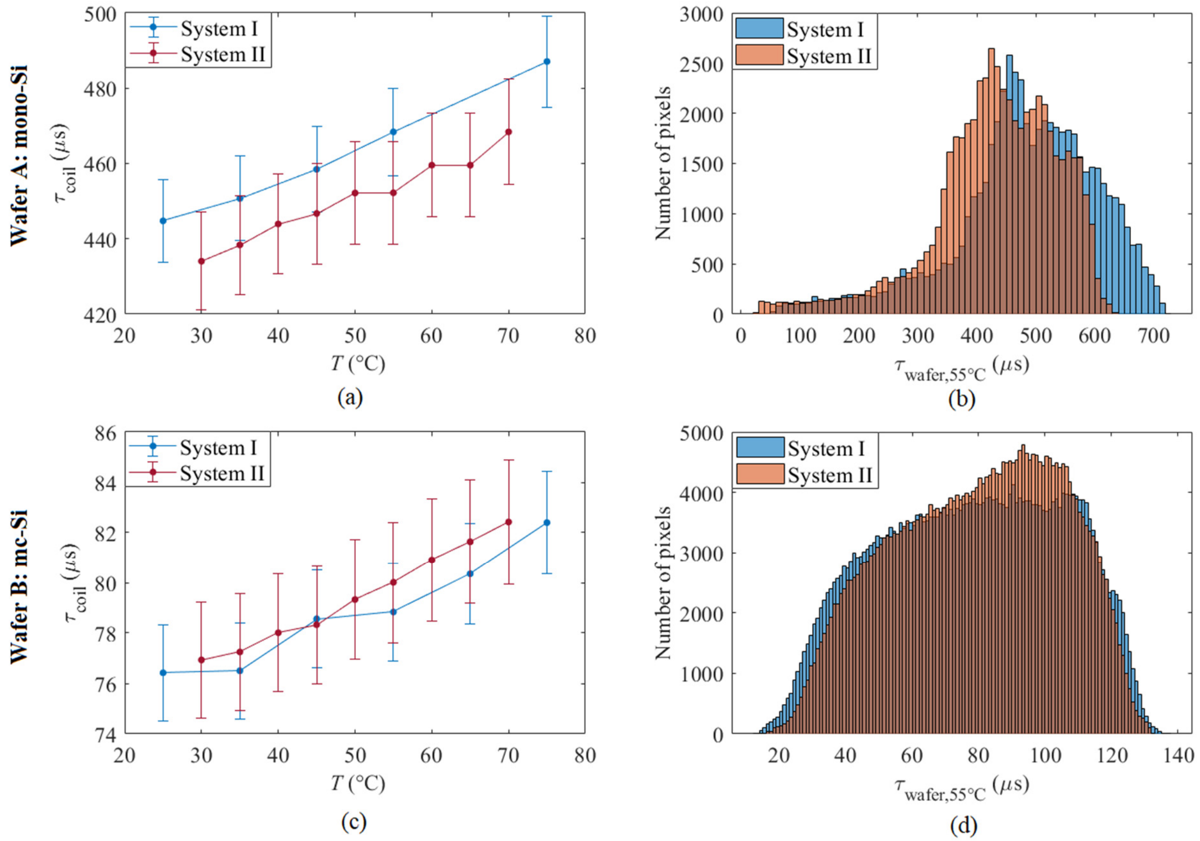

FIGURE 2. Average τ_{eff} in the PC coil area of the PL images of (a) Wafer A and (b) Wafer B measured using Systems I and II at various temperatures; (c) lifetime histogram of Wafer A and (d) Wafer B measured using both Systems I and II at 55°C.

is built into System I, the calibration is performed based on the correct location on the wafer. This reduces uncertainties arising especially for non-uniform materials such as mc-Si wafers.

Temperature Sensitivity of Compensated Silicon Wafers

When investigating the temperature sensitivity of solar cells, average parameter values are often used. Most commonly, the temperature sensitivity of V_{oc} is quantified using $\beta_{V oc}$ defined in Eq (4) [11]. As demonstrated in Ref. [6], a large variation of this parameter can be found across a wafer which suggests that spatial analysis is important for an in-depth analysis.

To illustrate the usefulness of our procedure for characterization of more complex materials, and for understanding the temperature sensitivity of iV_{oc} across different wafers, the method is applied to two compensated mc-Si wafers originating from the bottom and the top of a central brick. Images of the relative $\beta_{iV oc}$ (Eq. (4), normalized to iV_{oc} at 25°C at each pixel) of Wafers C and D are shown in Figs. 3(b) and (e), respectively. Large variations are found across both wafers, however, the non-uniformity is more pronounced for Wafer D. This wafer mostly shows a lower temperature sensitivity than Wafer C and additionally contains small areas with much lower sensitivity than the rest of the wafer [bright areas in Fig. 3(e)].

To correlate $\beta_{iV oc}$ with material quality and recombination mechanisms, maps of iV_{oc} and γ are shown in Figs. 3(a) and (c) for Wafer C and Figs. 3(d) and (f) for Wafer D. A region of interest (ROI) is selected on Wafer D exhibiting reduced temperature sensitivity. Comparing Figs. 3(d) and (e), the ROI can be identified as a low-quality area on the wafer containing patches with reduced iV_{oc}. This is surprising, since Eq. (4) predicts low iV_{oc} areas to result in an

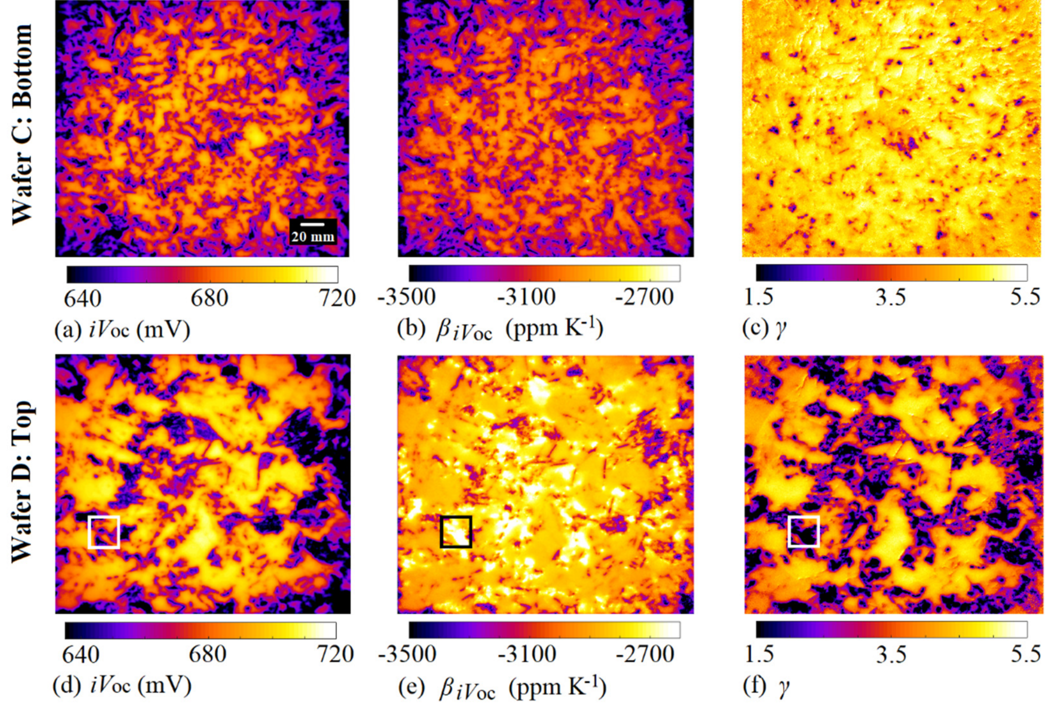

FIGURE 3. Images of iV_{oc} at room temperature, $\beta_{iV_{oc}}$, and γ of two compensated mc-Si wafers from (a-c) the bottom and (d-f) the top of a central brick. The wafers were characterized using System I.

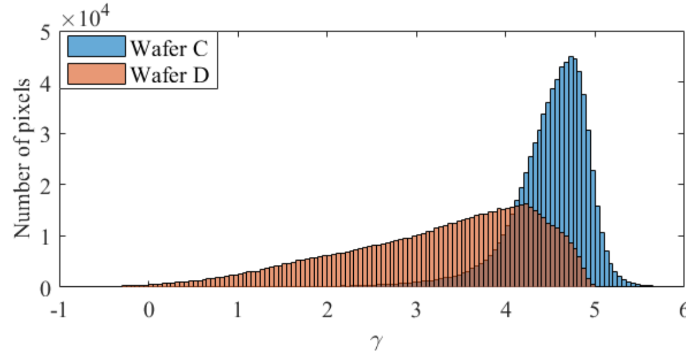

FIGURE 4. Histograms of γ values for Wafers C (bottom wafer) and D (top wafer).

increased temperature sensitivity, as is the case on other areas on the wafer. Turning our attention to Fig. 3(f), the ROI is found to originate from an area with γ values sufficiently low to counteract the reduced iV_{oc}, resulting in lower temperature sensitivity in that specific area.

To examine the spatial distribution of γ values across the Wafers C and D, Fig. 4 shows histograms of the number of pixels with different γ values. Wafer D is found to show a considerably larger variation in γ values across the wafer compared to Wafer C. This indicates that different recombination centers are limiting the two wafers and influencing their temperature sensitivity.

SUMMARY

In this paper, we presented a novel calibration routine for temperature dependent PL imaging based on a direct measurement of the PC of a wafer during image acquisition. This allows for the calibration constant to be obtained in true steady-state under similar temperature and illumination conditions as the PL image, resulting in a high-precision calibration with only few assumptions. The method was verified through comparison with a similar PL imaging system

with a different calibration process based on conventional flash-based QSS-PC measurement performed on a separate system. Good agreement was found between the two measurement systems when analyzing both a mono-Si and a mc-Si wafer and the proposed method can be considered a further development of existing procedures, however, with a more robust calibration routine.

Finally, the method was applied to two compensated mc-Si wafers from different brick positions to demonstrate the usefulness of our technique for characterizing more complex materials. Large variations in temperature sensitivity and γ values were found across the wafers. An area with low temperature sensitivity was investigated and surprisingly identified as a low-iV_{oc} area on the wafer, indicating that the temperature sensitivity in that specific area is determined by a recombination mechanism with a low γ value. The two wafers were found to exhibit different γ values, indicating that the wafers must be different recombination centers limiting the two wafers and influencing their temperature sensitivity.

ACKNOWLEDGMENTS

The authors would like to thank Jan Ove Odden (REC Solar Norway), Daniel Chung (UNSW), and Kyung Kim (UNSW) for providing wafers for the study; and SIRF (UNSW) and Rune Søndenå (IFE) for passivating the wafers.

REFERENCES

1. T. Trupke, R. A. Bardos, M. C. Schubert, and W. Warta, Appl. Phys. Letters **89**, 44103-44107 (2006).
2. J. A. Giesecke, M. C. Schubert, B. Michl, F. Schindler, and W. Warta, Sol. Energy Mater Sol. Cells **95** (3), 1011-1018 (2011).
3. Z. Hameiri, M. K. Juhl, R. Carlaw, and T. Trupke, "Spatially resolved lifetime spectroscopy from temperature-dependent photoluminescence imaging", in *Proceedings of IEEE 42nd Photovoltaic Specialist Conference,* 2015, pp. 1-3.
4. L. E. Mundt, M. C. Schubert, J. Schon, B. Michl, T. Niewelt, F. Schindler, and W. Warta, IEEE J. Photovolt. **5** (5), 1503-1509 (2015).
5. H. Haug, R. Søndenå, M. S. Wiig, and E. S. Marstein, Energy Procedia **124**, 47-52 (2017).
6. R. Eberle, S. T. Haag, I. Geisemeyer, M. Padilla, and M. C. Schubert, IEEE J. Photovolt. **8** (4), 930-936 (2018).
7. O. Dupré, R. Vaillon, and M. A. Green, *Thermal Behavior of Photovoltaic Devices: Physics and Engineering* (Springer, Cham, Switzerland, 2017), pp. 2-11.
8. T. Trupke, M. A. Green, P. Würfel, P. P. Altermatt, *et al.*, J. Appl. Phys. **94**, 4930-4937 (2003).
9. Sinton Instruments. WCT-120TS product note.
10. R. Sinton, and A. Cuevas, Appl. Phys. Lett. **69**, 2510 (1996).
11. M. A. Green, K. Emery, and A. W. Blakers, Electron. Lett. **18** (2), 97-98 (1982).